Cell

Visualizing GroEL/ES in the Act of Encapsulating a Folding Protein

Dong-Hua Chen,[1] Damian Madan,[2,6,7] Jeremy Weaver,[3,6] Zong Lin,[2,8] Gunnar F. Schröder,[4,5] Wah Chiu,[1,*] and Hays S. Rye[3,*]

[1]Verna and Marrs McLean Department of Biochemistry and Molecular Biology, National Center for Macromolecular Imaging, Baylor College of Medicine, Houston, TX 77030, USA
[2]Department of Molecular Biology, Princeton University, Princeton, NJ 08544, USA
[3]Department of Biochemistry and Biophysics, Texas A&M University, College Station, TX 77845, USA
[4]Department of Structural Biochemistry, Institute of Complex Systems (ICS-6), Forschungszentrum Jülich, 52425 Jülich, Germany
[5]Department of Physics, Heinrich-Heine Universität, 40225 Düsseldorf, Germany
[6]These authors contributed equally to this work
[7]Present address: Intellectual Ventures Laboratories, 1555 132nd Avenue Northeast, Bellevue, WA 98005, USA
[8]Present address: Department of Biotechnology and Biomedicine, Yangtze Delta Region Institute of Tsinghua University, Jiaxing, Zhejiang 314006, China
*Correspondence: wah@bcm.edu (W.C.), haysrye@tamu.edu (H.S.R.)
http://dx.doi.org/10.1016/j.cell.2013.04.052

SUMMARY

The GroEL/ES chaperonin system is required for the assisted folding of many proteins. How these substrate proteins are encapsulated within the GroEL-GroES cavity is poorly understood. Using symmetry-free, single-particle cryo-electron microscopy, we have characterized a chemically modified mutant of GroEL (EL43Py) that is trapped at a normally transient stage of substrate protein encapsulation. We show that the symmetric pattern of the GroEL subunits is broken as the GroEL *cis*-ring apical domains reorient to accommodate the simultaneous binding of GroES and an incompletely folded substrate protein (RuBisCO). The collapsed RuBisCO folding intermediate binds to the lower segment of two apical domains, as well as to the normally unstructured GroEL C-terminal tails. A comparative structural analysis suggests that the allosteric transitions leading to substrate protein release and folding involve concerted shifts of GroES and the GroEL apical domains and C-terminal tails.

INTRODUCTION

Many essential proteins fold only when assisted by ATP-powered machines known as molecular chaperones (Hartl et al., 2011). The GroEL/ES system of *Escherichia coli* is a well-studied example of the chaperonin class of molecular chaperones (Horwich and Fenton, 2009; Lin and Rye, 2006). GroEL is a tetradecamer of 57 kDa subunits, arranged as two stacked, seven-membered rings, each containing a large, solvent-filled cavity (Braig et al., 1994). The cavity-facing surface of the apical domain of each subunit is lined with hydrophobic amino acids that tightly bind substrates that are neither random coil nor natively folded proteins (so-called nonnative proteins; Fenton et al., 1994). Efficient folding of proteins that strictly depend on GroEL (so-called stringent substrate proteins) requires encapsulation of the nonnative substrate protein within a cavity formed by GroEL plus the smaller, ring-shaped cochaperonin GroES (Mayhew et al., 1996; Rye et al., 1997; Weissman et al., 1995, 1996). Encapsulation seals the GroEL cavity and results in the release of the substrate protein into an enlarged GroEL-GroES chamber (a *cis* complex). Upon release, folding is initiated and continues for a brief period, until the cavity is disassembled and the protein, folded or not, is ejected back into free solution (Mayhew et al., 1996; Todd et al., 1994; Weissman et al., 1994, 1995, 1996).

Encapsulation and initiation of folding ultimately depend upon ATP-driven structural rearrangements (Chen et al., 1994; Roseman et al., 1996; Rye et al., 1999). ATP binding to GroEL equatorial domains results in large, cooperative rearrangements, which elevate and rotate the apical domains (Burston et al., 1995; Xu et al., 1997; Yifrach and Horovitz, 1995). Exposed sites bind GroES, which results in a switch of the apical-domain surfaces from hydrophobic to polar (Xu et al., 1997), a switch believed to be essential for releasing substrate and triggering folding. Whereas protein folding is initiated inside the GroEL-GroES cavity, the relatively short lifetime of this complex limits the amount of time a protein has to fold (Burston et al., 1995; Rye et al., 1999; Todd et al., 1994; Weissman et al., 1994). The timer for complex disassembly is set by the rate of ATP hydrolysis within the *cis* cavity, ranging from 4–20 s, depending on temperature and the concentration of nonnative substrate protein (Burston et al., 1995; Grason et al., 2008; Rye et al., 1999).

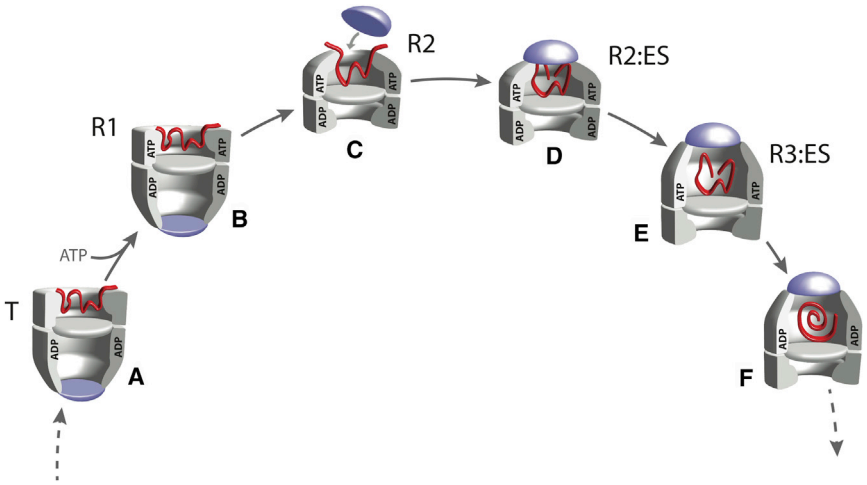

Figure 1. The GroEL Protein Folding Cycle Involves a Series of Allosteric Transitions within the Chaperonin Complex

(A–F) Nonnative substrate proteins enter the GroEL reaction cycle by binding to the open *trans* ring of an asymmetric GroEL-GroES complex, pulling the *trans* ring into the high-affinity "T" state (A; for cycle details, see Cliff et al., 2006; Horwich and Fenton, 2009; Lin and Rye, 2006). Protein encapsulation is initiated by highly cooperative binding of ATP to the *trans* ring, populating the R1 state (B), a conformational state of the GroEL ring with high affinity for the nonnative protein, but not yet for GroES. The R2 state (C) retains substantial, though weakened, affinity for the nonnative protein, binds GroES, and encapsulates the substrate protein (D). Transitions into or between the R1 and R2 states are also linked to disassembly of the GroEL-GroES complex on the opposite ring. The ATP-bound GroEL-GroES complex has a high affinity for GroES in the R3 state (E), which releases the nonnative substrate protein into the enclosed *cis* cavity, to initiate folding. Hydrolysis of ATP within the *cis* ring triggers a transition of the complex to at least one additional conformational state (F).

Recent structural work provides insight into how a nonnative substrate protein is bound to an open GroEL ring and a view of a fully folded protein inside the GroEL cavity (Clare et al., 2009; Elad et al., 2007; Falke et al., 2005, Kanno et al., 2009), but structural information about nonnative proteins during and immediately following encapsulation, the point at which folding is initiated, remains limited. In fact, the cooperative structural transitions of the GroEL ring that occur in response to ATP binding appear to create a paradox. Given that nonnative substrate proteins and GroES are thought to bind to overlapping sites on the GroEL apical domains, how is it possible for ATP binding to drive a GroEL ring into a state with high affinity for GroES without causing premature release of the folding intermediate outside the chaperonin?

Binding competition between GroES and a substrate protein to the apical domains could be avoided if the ATP-bound GroEL ring populates an intermediate conformation that transiently binds both substrate protein and GroES (Cliff et al., 2006). Entry into and exit from such a state would require an orderly allosteric cascade designed to enforce a specific ligand binding sequence (Clare et al., 2012; Cliff et al., 2006; Madan et al., 2008; Ueno et al., 2004). The sequence begins with the nonnative substrate protein binding to the open *trans* ring of an asymmetric GroEL-GroES complex with high affinity for the substrate protein but without significant affinity for GroES (Figure 1A; Lin et al., 2008). Cooperative binding of ATP to the same GroEL ring is then thought to initiate encapsulation through a series of conformational states, which sequentially weaken the interaction between GroEL and the substrate protein, while simultaneously strengthening the interaction with GroES (Figures 1B–1F). Whereas functional and kinetic studies strongly suggested the existence of such an allosteric cascade, because they are only transiently populated, the structural nature of these key intermediate states has remained poorly understood. A recent cryo-electron microscopy (cryo-EM) study of GroEL in the presence of ATP has begun to fill in some of these missing details, by successfully classifying several intermediate conformations of the GroEL apical domains (Clare et al., 2012). This study provides structural evidence for a sequential allosteric cascade, as well as insight into the intermediates populated by an ATP-bound GroEL ring prior to encapsulation. However, the absence of GroES and nonnative substrate protein in these studies leaves unresolved the key structural transitions that lead to substrate protein encapsulation, release, and folding.

Here, we show a nonnative substrate protein trapped inside the GroEL-GroES cavity during encapsulation. We used cryo-EM and single-particle three-dimensional (3D) reconstruction to determine the structure of a chemically modified GroEL mutant, which stalls in an allosteric state just prior to substrate protein release (the R2 state; Madan et al., 2008). Population of this normally transient state requires a break in the 7-fold rotational symmetry of the GroEL ring. As the GroES heptamer engages the GroEL ring to seal the cavity, the nonnative protein contacts the lower segment of the GroEL apical domains. Strikingly, the normally unstructured C-terminal tails of the GroEL subunits extend up from the base of the cavity to make extensive contact with the nonnative protein. Removal of the C-terminal tails results in an increase in premature substrate protein release prior to GroES binding. Efficient encapsulation thus requires an intermediate conformation of the GroEL-GroES complex that simultaneously binds both the nonnative protein and GroES.

RESULTS

Cryo-EM of a Functionally Trapped GroEL (EL43Py)-GroES Complex

Previous work showed that the GroEL variant EL43Py is a potent tool for examining the linkage between substrate protein encapsulation, release, and folding (Madan et al., 2008). EL43Py was created through homogeneous N-1-pyrene maleimide alkylation of a surface-exposed Cys residue engineered into a stem-loop at the bottom of the GroEL cavity. EL43Py encapsulates nonnative substrate proteins beneath GroES but only very slowly releases them into the GroEL-GroES cavity to initiate folding. The EL43Py variant thus provides an excellent opportunity to trap and structurally characterize a key conformation of the GroEL-GroES

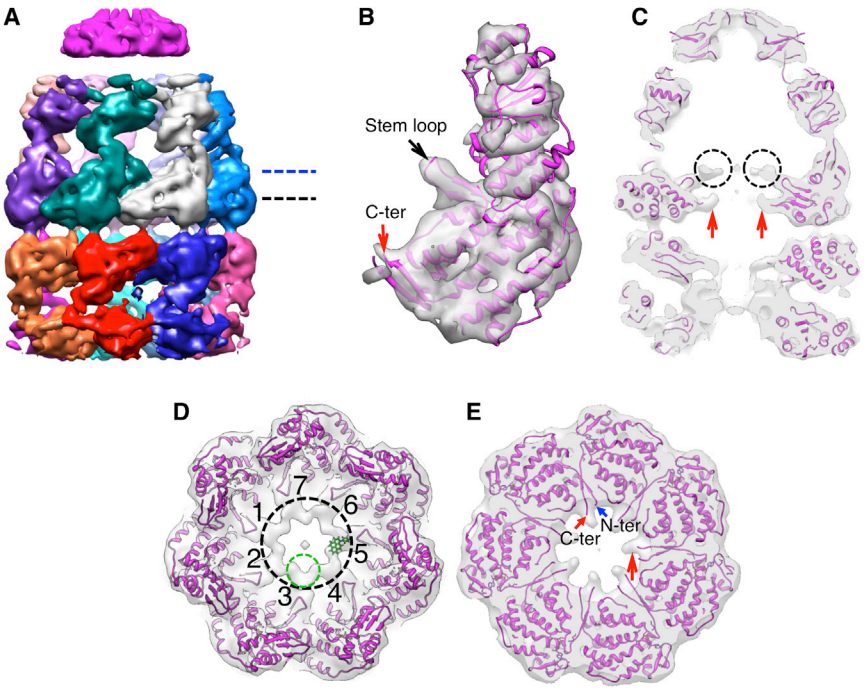

Figure 2. The Structure of the EL43Py398A-GroES-ATP Complex Determined at 8.9 Å Resolution by Cryo-EM with C7 Symmetry Imposed

(A) Side view of the EL43Py398A-GroES-ATP density map displayed at a contour level of 1.3 σ. Individual GroEL subunits are shown in different colors; GroES is magenta. All other density maps shown in this study are displayed at a contour level of 1.0 σ (unless otherwise noted).

(B) Close-up view of a single EL43Py398A *cis*-ring subunit (contour level of 1.5 σ) overlapped with a rigid-body, flexibly refined fit of the GroEL-GroES-ADP crystal structure (PDB ID code 1AON; magenta) using the program DireX (Schröder et al., 2007). The stem loop containing Cys 43 and the GroEL C terminus are labeled with arrows.

(C) A medial slice of the density map shown in (A), with the density rendered transparent and superimposed on a rigid-body, flexibly refined fit of the GroEL-GroES-ADP crystal structure. In (C), extra density is visible at the tips of the equatorial stem loops of each GroEL subunit (amino acids 34–52; black dashed circles). The observed densities beyond amino acid 525 in the C-terminal tails are indicated by red arrows.

(D) The additional stem-loop density for each subunit is shown (inside of black dashed circle), viewed from above, at a slice level indicated by the dashed blue line in (A). The seven stem loops are labeled 1–7, respectively. A single N-1-pyrene maleimide dye molecule (green) was rigid-body fit into the density at the tip of one stem loop in the EL43Py398A-GroES-ATP complex using Chimera.

(E) View of the *cis*-ring equatorial domain near the subunit C termini, viewed from above, at the slice level indicated by the black dashed line in (A). Substantial density (large red arrow) is visible in the region of the subunit C termini, well beyond the last crystallographically resolved residue (small red arrow). The position of the GroEL subunit N terminus is indicated by the blue arrow.

See also Figures S1 and S7.

complex that is essential for substrate protein encapsulation but is normally highly transient (the GroES-bound R2 state of the GroEL ring; Figure 1D). In order to facilitate this study, we incorporated one additional modification into the EL43Py background, introducing a well-established mutation (D398A) that prevents ATP hydrolysis by GroEL, without affecting ATP or GroES binding (Rye et al., 1997). EL43Py398A stalls at the same point in the allosteric cycle as EL43Py (Figure S1A available online) but cannot hydrolyze ATP (data not shown). Using EL43Py398A and limiting amounts of ATP and GroES, we were thus able to create a chaperonin sample enriched in asymmetric EL43Py398A-GroES-ATP complexes (a so-called ATP bullet complex) with the *cis* cavity trapped in the R2 configuration. Cryo-EM was used to image this sample (Figure S1B), which contains multiple molecular species even when using an optimized mixing protocol, because the assembly reaction can never be driven to completion to yield a single, unique EL43Py398A-GroES-ATP bullet complex.

We applied a consecutive multiple-model refinement strategy, previously used to successfully analyze images of chaperonins with mixed conformations and compositions (Chen et al., 2006, 2008; Cong et al., 2012). The first round of processing of 71,200 particle images yielded three subpopulations of images that resulted in free GroEL tetradecamer (no GroES bound), bullet-shaped GroEL-GroES complexes (with GroES bound to only one end of the GroEL tetradecamer) and football-shaped GroEL-$GroES_2$ complexes (with GroES bound to both ends of the GroEL tetradecamer). Because we were only interested in the structure of the bullet-shaped complex in the present study, we did not pursue a structural determination of the other subpopulations.

The subset of images corresponding to the bullet-shaped complex was subjected to several additional rounds of multiple-model refinement to yield a final homogeneous data set of 8,372 bullet-shaped particle images. This final data set was split into two halves for a gold-standard resolution assessment (Scheres and Chen, 2012). A 3D structure of the bullet complex at ~8.9 Å was reconstructed using C7 symmetry (Figures 2A and S1C) from all 8,372 highly selected particle images. A symmetry-free reconstruction from the same set of 8,372 highly selected particle images was also obtained at 13.9 Å resolution. Without a symmetry imposition, the subunits are not perfectly symmetrically arranged but do not deviate far from 7-fold symmetry (data not shown). Because the symmetry-free map is close to C7 symmetry, and the symmetry imposition generated a higher resolution map, we employed the symmetry-imposed map for subsequent structural analysis.

The structures of the wild-type GroEL-GroES-ADP complex and the EL43Py398A-GroES-ATP complex bear substantial similarities at ~9 Å resolution, except in three locations. First, the position of the GroEL apical domains and the orientation of GroES are slightly shifted in the EL43Py398A-GroES-ATP complex (an R2-ES complex; see below). Second, substantial additional density protrudes into the chaperonin cavity from the end of a

stem loop (amino acids 34–52) at the base of the EL43Py398A-GroES *cis* cavity (Figures 2B–2D and S1D). This density emanates in part from the expected attachment point of the pyrene dyes at position 43, which resides at the tip of the stem loop (Figure 2B). However, the density near this position (green dashed circle) is larger than can be accounted for by the dye molecule alone (Figure 2D). Third, significant density rises up from the bottom of each GroEL subunit (large red arrow in Figures 2C, 2E, and S1E), beyond the last crystallographically resolved residue at position 525, toward the dye attachment position. The location of this additional density is consistent with the normally flexible C-terminal tails of the GroEL subunits, which extend from residue 526 to the C terminus (a total of 23 amino acids), rising from the bottom of the GroEL subunits and interacting with the pyrene dyes attached to the protruding stem loop (Figures 2C, 2D, and S1E). Additional density is also apparent in the *trans* ring of the complex (Figure S1E), though the density in this ring is somewhat more complex than that observed in the *cis* ring and may suggest that the GroEL C-terminal tails in the *trans* ring make contact with both the pyrene dyes and the apical domains.

Visualizing an Encapsulated Nonnative Protein

We next examined the conformation of the EL43Py398A-GroES-ATP complex in the presence of a nonnative substrate protein. To accomplish this goal, we modified our original preparation protocol to add the well-characterized GroEL-dependent substrate protein RuBisCO (see the Experimental Procedures). In brief, EL43Py398A was first mixed with nonnative RuBisCO to form a binary complex. The EL43Py398A-RuBisCO binary complex was then mixed with limiting ATP and GroES, which results in the formation of multiple species, including the bullet-shaped EL43Py398A-RuBisCO-GroES-ATP complex, both with and without nonnative RuBisCO inside the *cis* chamber. After cryo-EM imaging (Figure S2A) and heterogeneity sorting of the particle images, we examined the first of two major subpopulations of bullet-shaped particle images, which were used to produce both symmetry-imposed and symmetry-free maps. The symmetry-imposed map for this RuBisCO-free subpopulation, which is devoid of density within either *cis* or *trans* cavities (Figures S2B and S2C), is very similar to that of the empty EL43Py398A-GroES-ATP complex (Figure 2A). Additionally, the unwrapped density in the symmetry-free reconstruction from the same set of RuBisCO-free particle images shows that the complex retains 7-fold symmetry (Figure S2D).

We examined the second major subpopulation of bullet-shaped particle images to generate a 9.2 Å symmetry-free reconstruction of the bullet-shaped complex (Figures 3A and S3A). Remarkably, this map displays strong density within the *cis* cavity, most likely from the nonnative RuBisCO monomer trapped within the stalled R2 complex (gold in Figure 3A). The estimated mass of the visible RuBisCO monomer at a contour level of 1.0 σ is ~35 kDa, representing roughly 70% of the native RuBisCO monomer mass, assuming the central density comes from the RuBisCO alone. However, no regular secondary structural elements could be defined in the putative RuBisCO density either visually or quantitatively (based on SSEHunter; Baker et al., 2007), and no fragment of the RuBisCO crystal structure could be docked convincingly into the density.

The presence of the nonnative RuBisCO within the R2 cavity also alters the structure of the GroEL-GroES complex itself. The rotational symmetry of the EL43Py398A apical domains, on both the *cis* and *trans* rings, is broken in the presence of nonnative RuBisCO (Figures 4A–4C and S3B), with a gap appearing between the apical domains of two *cis*-ring neighboring subunits (Figures 4A and 4C). Interestingly, the point at which the *cis* ring appears to break 7-fold rotational symmetry coincides with direct physical interaction between the nonnative RuBisCO monomer and the lower segment of the apical domains of two *cis* ring subunits (Figures 3B–3D and 4C and 4D). The reliability of this connecting density is substantiated by its low variance in the 3D variance analysis from 100 reconstructed maps with different subsets of particle images (red in Figure 3D). The *cis*-ring equatorial domains also deviate slightly from C7 symmetry, which can be observed as differences in the separation of the equatorial domain helices between different subunits (Figure S3C).

A Role for the GroEL C-Terminal Tails in Protein Encapsulation

A second striking feature of the R2 state revealed by the EL43Py398A-RuBisCO-GroES-ATP complex is a direct, physical contact between the nonnative RuBisCO monomer and density from the base of the GroEL cavity wall (Figures 3B, 3C, 4E, and S3D). This interaction site is principally in the region of the dye-modified stem loops near amino acid 43, and some of this interaction is probably due to contact between the pyrene dyes and the nonnative substrate protein (Figure S3D). However, in the absence of RuBisCO, substantial density from the GroEL C termini is also present in this region (Figures 2C, 2E, and S1E). Several studies have suggested that the C-terminal tails of the GroEL subunits play important, though poorly defined, roles in protein folding and regulation of the GroEL ATPase cycle (Farr et al., 2007; Machida et al., 2008; McLennan et al., 1993; Tang et al., 2006). Additionally, 3D variance analysis of the EL43Py398A-RuBisCO-GroES-ATP structure suggests a direct and heterogeneous interaction between the nonnative RuBisCO and the C-terminal region of the GroEL subunits (Figure 3D). By far some of the largest 3D variance in the GroEL subunits in the EL43Py398A-RuBisCO-GroES-ATP complex appears around the equatorial domains, in regions near or containing the C-terminal tails of the GroEL subunits. Whereas high-variance regions (red in Figure 3D) are observed on both the *cis* and *trans* rings, in the *cis* ring these regions appear to be in intimate contact with the nonnative substrate protein (Figure 3D). The putative RuBisCO density also displays high variance, suggesting that the nonnative protein remains conformationally heterogeneous at this stage of the GroEL reaction cycle.

We next considered whether the observed contacts between the C-terminal tails and nonnative RuBisCO require the presence of the pyrene dyes. Using a mixing protocol similar to that described above, we created a population of asymmetric complexes using the GroEL variant D398A (EL398A) that does not contain the pyrene dye. Following imaging (Figure S4A) and heterogeneity sorting, the bullet-shaped structure of the EL398A-RuBisCO-GroES-ATP complex with RuBisCO within the *cis* cavity was solved to 15.9 Å without imposing a symmetry

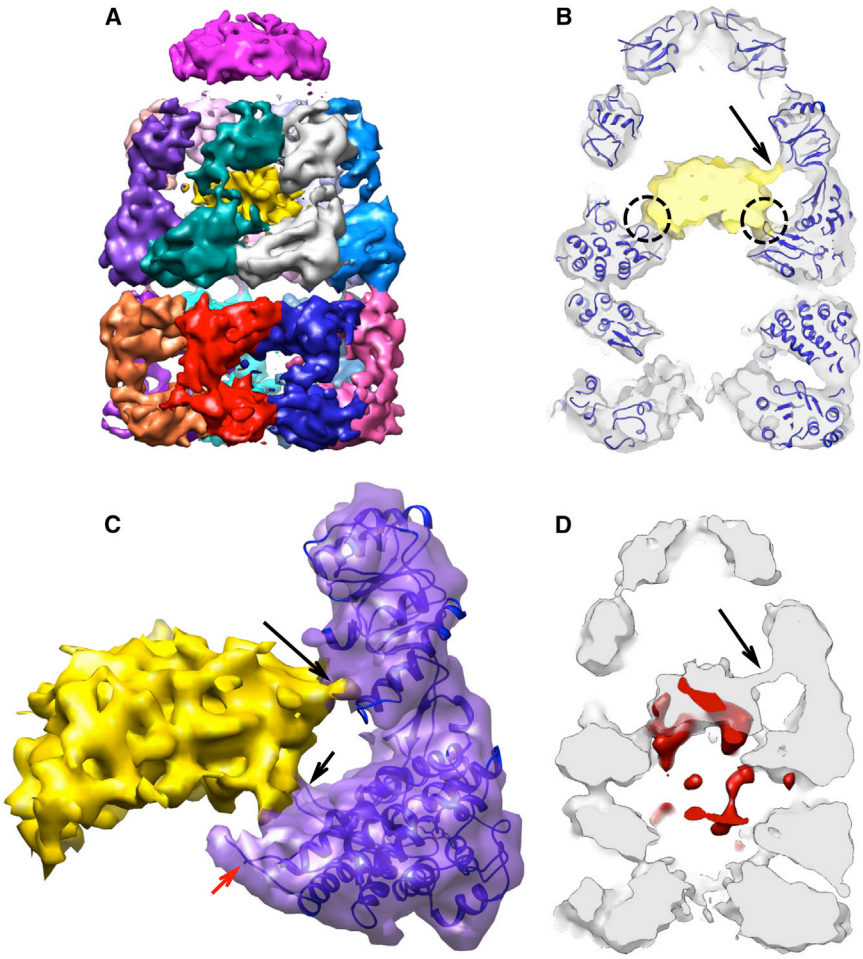

Figure 3. The Structure of the EL43Py398A-GroES-ATP Complex Containing Nonnative RuBisCO within the *cis* Cavity Determined at 9.2 Å by Cryo-EM without Imposed Symmetry

(A) A side view of the density map of EL43Py398A-RuBisCO-GroES-ATP complex (contour level 1.23 σ) shown colored as in Figure 2, with density from the encapsulated, nonnative RuBisCO monomer shown in gold.

(B) A medial slice of the EL43Py398A-RuBisCO-GroES-ATP complex with the density rendered transparent and overlapped with a rigid-body, flexibly refined fit of the GroEL-ADP-GroES crystal structure (PDB ID code 1AON) to the cryo-EM map. Additional density around the GroEL equatorial domain stem loops makes direct contact with the nonnative RuBisCO monomer (dashed black circles). The RuBisCO is also in contact with the lower region of the apical domain of one *cis*-ring GroEL subunit in the region of F281 (black arrow).

(C) A close-up view of one *cis*-ring GroEL subunit in direct contact (long black arrow) with the nonnative RuBisCO monomer (gold; contour level of 1.05 σ). The GroEL subunit stem loop (short black arrow) and C terminus (red arrow) are indicated.

(D) A medial slice of the variance map derived for the EL43Py398A-RuBisCO-GroES-ATP complex (red; see the Experimental Procedures) is shown overlapped with the average map of the complex (gray; orientation as in B), calculated from 100 3D reconstructions of the complex computed during the variance calculations. The largest variations in the density map are from the nonnative RuBisCO monomer and cavity-facing regions of the GroEL equatorial domains, most likely the C termini of the *cis* and *trans* rings.

See also Figures S2, S3, and S7.

constraint (Figures 5 and S4B). Because the EL398A-GroES complex does not stall in the R2 state, but productively releases the substrate into the *cis* cavity and initiates folding, though it cannot hydrolyze its bound ATP (Rye et al., 1997), the EL398A-RuBisCO-GroES-ATP complex constitutes a substrate-occupied R3 state of the *cis* ring (Figure 1E).

Once again, a substantial amount of density from the RuBisCO monomer is visible within the *cis* cavity (Figure 5B). The apparent mass of the RuBisCO monomer in this complex appears to be less than that in the EL43Py398A-RuBisCO-GroES-ATP structure (Figures 3B and S3D). This is likely due to the fact that the R3 cavity of the EL398A-GroES complex is fully folding active (Figure 1E), unlike the R2 cavity of the EL43Py398A-GroES complex (Figure 1D). Even though the EL398A complex was rapidly processed for cryo-EM freezing to prevent complete folding of the encapsulated RuBisCO, the initiation of folding in this complex could not be blocked at a specific step, as it is with EL43Py398A. The enclosed RuBisCO monomer will thus be a highly heterogeneous mix of both folded and nonnative states, resulting in a lower resolution reconstruction. The C-terminal tails of the GroEL subunits are also not resolved, because the map represents a heterogeneous ensemble of interactions between the RuBisCO monomer and the C-terminal tails. Nonetheless, a significant contact between the base of the GroEL cavity wall, in the region of the C-terminal tails and stem loop and the RuBisCO monomer is apparent (Figure 5B). To further validate this structure, a completely independent reconstruction of this structure with a different initial model in which the *cis* cavity was empty (a low-pass filtered X-ray structure of GroEL-GroES-ADP complex; Protein Data Bank [PDB] ID code 1AON) still converged well and displayed a very similar contact between the encapsulated RuBisCO and the GroEL C-terminal region and stem loops (Figure S4C). As expected for a released and folding competent RuBisCO monomer, this contact is less substantial than observed in the EL43Py398A complex (Figures 4E, 5B, and S3D) and, more importantly, does not depend upon the presence of the pyrene dyes.

The contact between the GroEL C-terminal tails and nonnative RuBisCO suggests that the C termini play a direct and important role in ensuring efficient substrate protein encapsulation beneath GroES. In order to test this hypothesis, we generated a GroEL variant with a C-terminal truncation at the last crystallographically resolved residue (ELΔ526). A similar truncation has been previously observed to display both perturbed ATPase activity

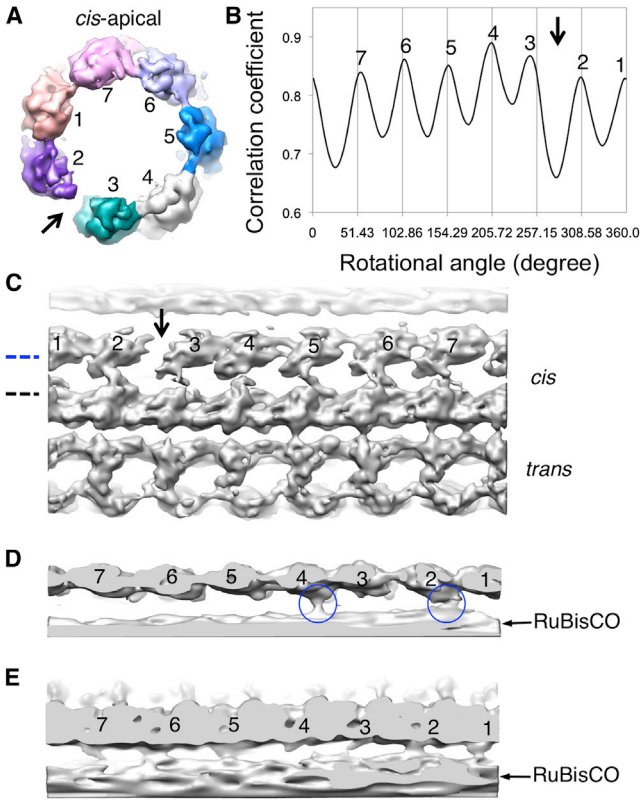

Figure 4. The C7 Symmetry of the GroEL *cis*-Ring Is Broken in the EL43Py398A-RuBisCO-GroES-ATP Complex Near Points of Contact between the Nonnative RuBisCO and the GroEL Cavity Wall

(A) *cis*-ring apical domains of the EL43Py398A-RuBisCO-GroES-ATP structure are shown as in Figure 3A, viewed from the top of the *cis* ring. A gap (black arrow) in the ring density is observed between subunit 2 (purple) and subunit 3 (dark cyan).

(B) The cross-correlation coefficient between the map of the *cis*-ring apical domains and a symmetric reference indicates that subunit 4 is closer to subunit 3, which is approximately 9° off its C7 symmetrical position, leaving a gap between subunits 3 and 2 (black arrow).

(C) The gap (black arrow) between the two neighboring GroEL subunits is shown in an unwrapped, planar display from the outside of the 9.2 Å density map of EL43Py398A-RuBisCO-GroES-ATP, as viewed from the side.

(D) Top view slice of the planar map, through the lower region of the *cis* ring apical domains (C, blue dashed line) shows interactions between the nonnative RuBisCO monomer and the lower aspect of the GroEL apical domains of subunits 2 and 4 (blue circles).

(E) Top view slice of the planar map through the upper section of the equatorial domains (C, dashed black line) indicates contacts with the GroEL subunits near the stem-loop region of the equatorial domain. The isosurface threshold for (D) and (E) is 0.9σ.

See also Figure S2.

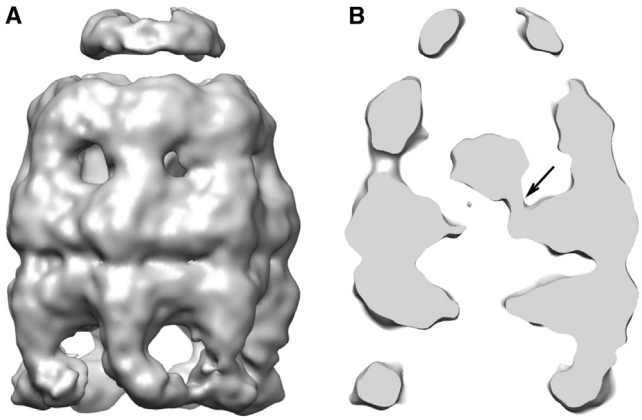

Figure 5. The Structure of the EL398A-GroES-ATP Complex Containing RuBisCO within the *cis* Cavity Determined at 15.9 Å by Cryo-EM Reconstruction without Imposed Symmetry

(A) A side view of the EL398A-RuBisCO-GroES-ATP density map.

(B) Medial slice of the EL398A-RuBisCO-GroES-ATP complex indicates direct contact between the folding RuBisCO monomer and the C-terminal and stem-loop region of one *cis*-ring GroEL subunit (black arrow).

See also Figures S4 and S7.

and a reduced ability to support folding of several model substrate proteins (Farr et al., 2007; Machida et al., 2008; Tang et al., 2006). We employed this GroEL variant in a gel filtration assay designed to score the efficiency of protein encapsulation (Figure 6A). When nonnative GFP is bound to the *trans* ring of a wild-type GroEL-GroES-ADP bullet, approximately half of the initially bound protein is encapsulated inside a new *cis* cavity upon the addition of limiting ATP (Figure 6B). However, when the GroEL C-terminal tails are removed in the ELΔ526 variant, the efficiency of GFP encapsulation beneath GroES drops dramatically (Figure 6C). Similar results are obtained when the same experiment is conducted with both nonnative rhodanese (Figure 6D) and RuBisCO (Figure 6E), though the drop in encapsulation efficiency is not as substantial.

Structural Changes in the GroEL-GroES Complex between the R2 and R3 States

Following GroES binding and substrate protein encapsulation, the R2 state of the GroEL-GroES complex must then execute a shift to the R3 state, whereupon the substrate protein is released into the GroEL-GroES cavity and folding is triggered (Figure 1). In order to gain additional insight into this transition, we re-examined our cryo-EM data using strongly restrained flexible fitting of the atomic model of the GroEL-GroES-ADP complex (PDB ID code 1AON) into our cryo-EM maps (Figures 2A, 3A, and 5A) with the program DireX (Schröder et al., 2007). The models generated from each flexible fitting analysis were then compared with each other in an attempt to isolate the conformational changes that lead from the R2 to the R3 state of the GroEL-GroES complex.

We first sought to identify structural differences between the R2 and R3 complexes that do not depend on the presence of the nonnative substrate protein. This was accomplished by comparing the EL43Py398A-GroES-ATP complex, representing an empty R2 complex, to a previously described EL398A-GroES-ATP complex (Ranson et al., 2006), representing, in principle, an empty R3 complex (Figure 1E). Surprisingly, the conformational differences between these two complexes are relatively small (Figures 7A–7C). The *cis* ring apical domains appear to display slight counterclockwise rotations (1°–2°) within the plane of the ring, but the overall position and elevation of the apical domains do not appear to change substantially (Figures

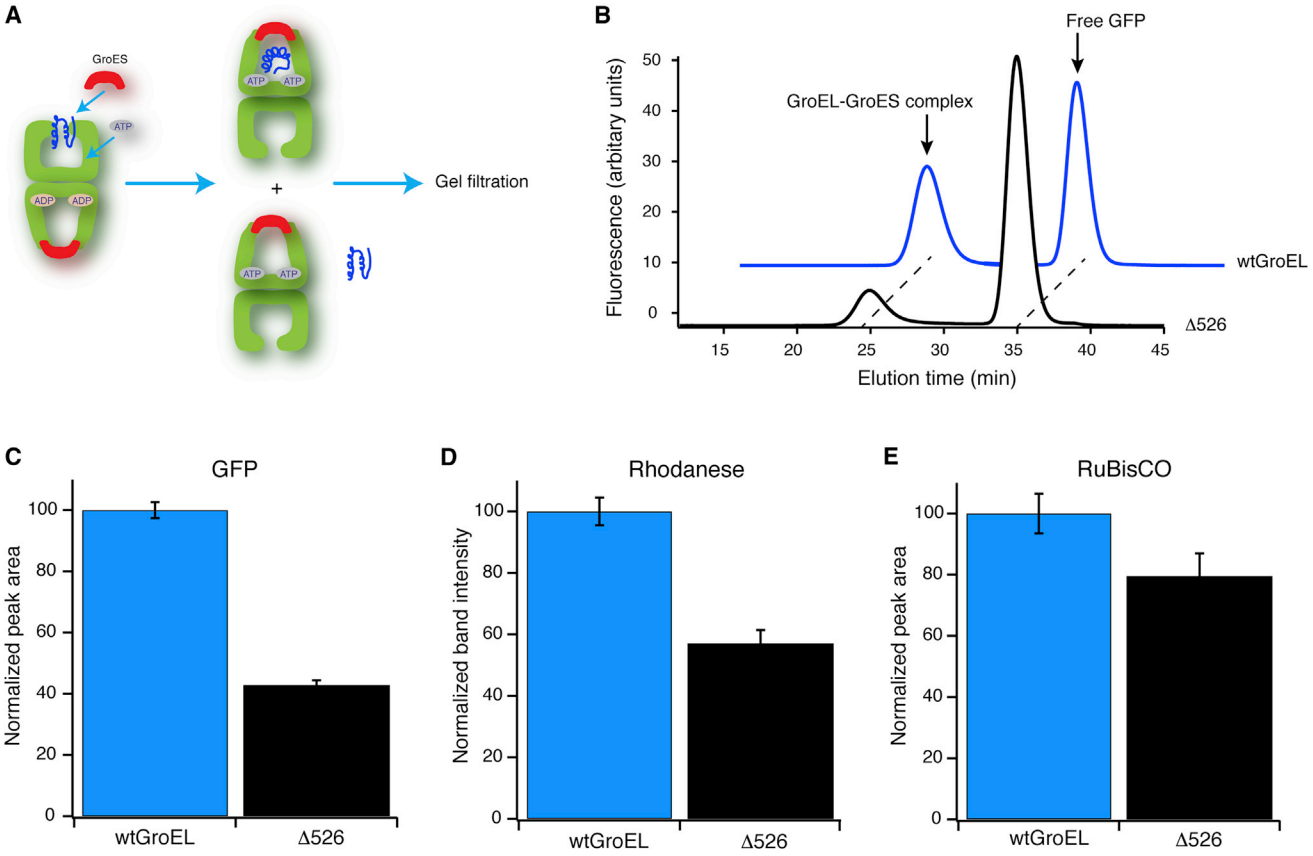

Figure 6. Removal of the GroEL C-Terminal Tails Results in Premature Substrate Protein Release and Reduced Encapsulation Efficiency

(A) Experimental schematic: nonnative substrate protein (blue) is bound to the open *trans* ring of a GroEL ADP bullet complex in the presence of excess GroES. Encapsulation is initiated by the addition of ATP. ATP binding and turnover is limited to a single round by addition of hexokinase and glucose within 10 s of ATP addition. Complexed and free substrate proteins are separated by gel filtration chromatography with an in-line fluorescence detector.

(B) Example of an encapsulation experiment using GFP as the substrate protein. The positions of encapsulated GFP (GroEL-GroES complex) and released GFP (free GFP) are indicated with arrows, for both wild-type GroEL (wtGroEL) and the Δ526 truncation mutant (Δ526).

(C–E) Encapsulation is quantitated for three independent substrate proteins: (C) GFP (normalized fluorescence peak area; n = 6), (D) Rhodanese (normalized SDS-PAGE band intensity by densitometry; n = 4), and (E) RuBisCO (fluorescently labeled; n = 6). The reduction in encapsulation of nonnative substrate protein by Δ526 GroEL relative to wtGroEL is robust: $p = 6.5 \times 10^{-9}$ for GFP, p = 0.0007 for rhodanese, and p = 0.0007 for RuBisCO (paired t test; error bars are one SD; see the Experimental Procedures for additional details).

7A and 7B). Likewise, the equatorial domains show almost no movement at the current resolution (Figure 7A). The position and conformation of the GroES heptamer also appears mostly unchanged (Figure S5A). The lack of substantial conformational differences between these two complexes suggests that either (1) the conformation we observe for the EL43Py398A-GroES-ATP complex is further along the R2-to-R3 transition than expected or (2) that the detailed conformational properties of either the R2 or R3 state are not observable or stable in the absence of the nonnative substrate protein.

To address these questions, we compared the empty R2 complex (EL43Py398A-GroES-ATP from Figure 2A) with the substrate protein occupied R2 complex (EL43Py398A-RuBisCO-GroES-ATP from Figure 3A). As shown in Figure S6, only slight differences between the two complexes are apparent, with the notable exception of the disruption of rotational symmetry and local structural shifts in the apical domains that make direct contact with the nonnative substrate protein. These observations suggest that the global conformation of the R2 state of the EL43Py398A *cis* ring is stable in the presence of the substrate protein.

We next examined whether conformational differences between an R2 and R3 complex can be detected when the *cis* cavity is occupied by a substrate protein. Strikingly, the substrate-occupied R3 complex (EL398A-RuBisCO-GroES-ATP from Figure 5) shows substantial rearrangements compared to the substrate-occupied R2 complex (EL43Py398A-RuBisCO-GroES-ATP from Figure 3; see Figure 7D–7F). The *cis* apical domains of the substrate-occupied R3 ring display sizable outward tilts and elevations (Figures 7D and 7E), increasing the cavity volume compared to the R2 ring, as well as shifting the position of the bound GroES heptamer upward (Figure 7D). This tilt and elevation are also associated with a small clockwise rotation of the apical domains within the plane of the ring (Figure 7E). The conformation of the bound GroES heptamer also changes, with the average position of the GroES subunits

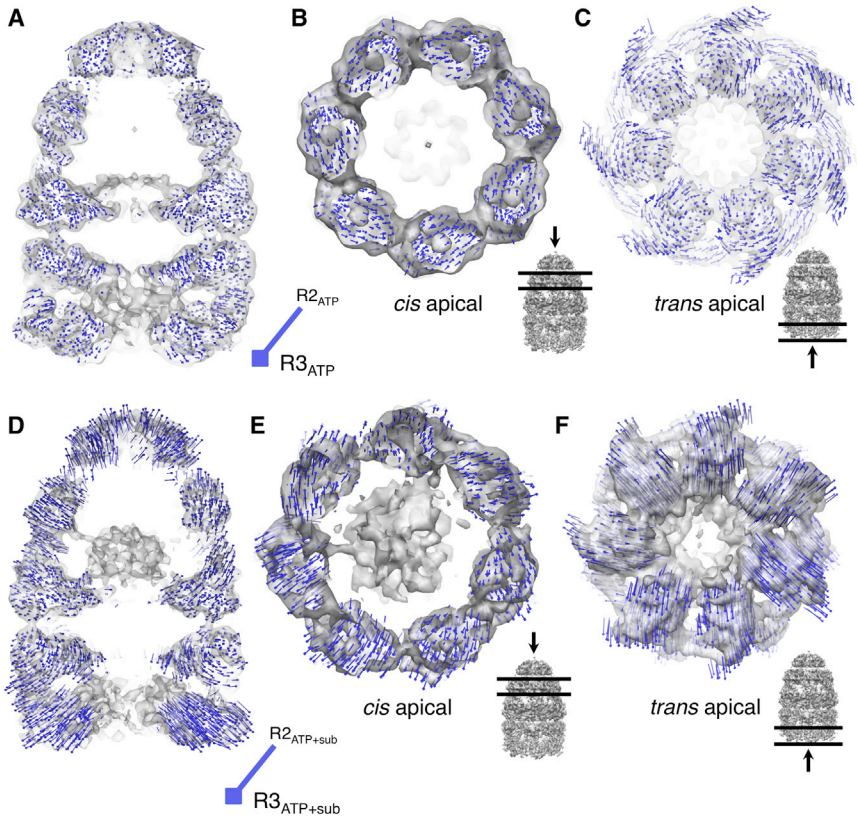

Figure 7. The Transition from the R2 to the R3 State in the Presence of RuBisCO Involves Large Structural Rearrangements of Both the *cis* and *trans* Rings

(A–C) Atomic models of the GroEL-GroES complex (PDB ID code 1AON) were refined against density maps of the empty EL43Py398A-GroES-ATP ($R2_{ATP}$; Figure 2A) and EL398A-GroES-ATP ($R3_{ATP}$; Ranson et al., 2006) complexes.

(D–F) Atomic models of the GroEL-GroES complex (PDB ID code 1AON) were refined against density maps of the EL43Py398A-RuBisCO-GroES-ATP complex ($R2_{ATP\ +\ sub}$; Figure 3A) and the EL398A-RuBisCO-GroES-ATP ($R3_{ATP\ +\ sub}$; Figure 5A). (A) Side view of the EL43Py398A-GroES-ATP density map: structural shifts associated with movement from an empty R2 complex to an empty R3 complex are illustrated with a field of difference vectors (blue lines and dots) to indicate the change in Cα positions from R2 (start) to R3 (end; square). Vector lengths are scaled by a factor of two to improve visibility. (B) View of structural changes in the *cis* apical domains and (C) *trans* ring apical domains. (D) Side view of the EL43Py398A-RuBisCO-GroES-ATP density map: structural shifts indicating the differences between the substrate-occupied R2 and R3 complexes. (E) View of structural changes in the *cis* apical domains and (F) the *trans* ring apical domains. For (B), (C), (E), and (F), the viewing direction and selected slice density are indicated by the black arrow and horizontal lines on the GroEL-GroES density map shown in the inset, to the lower right. In all cases, strongly restrained flexible model refinement was carried out with *DireX*. The designations R2 and R3 reference the functional allosteric states of the GroEL ring, illustrated in Figure 1.
See also Figures S5 and S6.

shifting outward in concert with the apical domains, resulting in a somewhat larger opening in the orifice at the top of the GroES dome (Figure S5B). The equatorial domains display only small movements, which are most notable as an outward shift in the region near the C termini (Figure 7D). The collective movements of the R3 *cis* ring thus appear poised to peel away the remaining contacts between the nonnative substrate protein and the apical domains and C-terminal tails. Notably, both release events occur once GroES is already bound. The final elevation and rotation of the apical domains in the R3 state are likely responsible for locking GroES into its highest affinity state for the ATP-bound GroEL ring (Cliff et al., 2006; Rye et al., 1997).

DISCUSSION

Conformational Properties of an Encapsulated Folding Intermediate

The structure of the EL43Py398A-RuBisCO-GroES-ATP complex provides a view of a protein folding intermediate inside of the GroEL-GroES cavity (Figure 3). Whereas earlier studies have visualized nonnative proteins bound to an open GroEL ring (Clare et al., 2009; Elad et al., 2007; Falke et al., 2005), as well as fully folded proteins inside the GroEL-GroES cavity (Clare et al., 2009; Kanno et al., 2009), the RuBisCO folding intermediate we describe here exists in transition between the two. Earlier work demonstrated that the RuBisCO monomer upon which GroEL operates is likely a middle- to late-stage protein folding intermediate (Lin and Rye, 2004; Lin et al., 2008; van der Vies et al., 1992), where the polypeptide chain has collapsed but is not as compact as the native state and which possesses significant secondary structure but poorly organized and highly heterogeneous tertiary structure. We examined the RuBisCO density in the EL43Py398A-RuBisCO-GroES-ATP complex for recognizable structural elements of native RuBisCO. Secondary structural elements should theoretically be identifiable in this structure, given the subnanometer resolution of the entire reconstruction. For example, helices in the equatorial domain of the GroEL subunits can be readily assigned (Figure S3C). However, our analysis failed to objectively identify any native state secondary structural elements. The lack of identifiable secondary structural elements in the putative RuBisCO region is consistent with the RuBisCO monomer populating a heterogeneous ensemble of collapsed and partially organized states (Figure 3A).

Coordinated Action of the GroEL Apical Domains and C Termini

Our results suggest that direct contact between nonnative substrate proteins and the C-terminal tails of the GroEL subunits helps prevent premature substrate protein escape during encapsulation beneath GroES. However, this interaction alone cannot

fully explain efficient encapsulation on an R2 ring. Indeed, most of the nonnative RuBisCO and rhodanese are still correctly captured in the absence of the C termini (Figures 6D and 6E), suggesting that contacts between the GroEL apical domains and nonnative RuBisCO must also play an important role. The structure of the R2 cavity in the EL43Py398A-RuBisCO-GroES-ATP complex provides strong evidence for this mechanism. As shown in Figures 3 and 4, the nonnative RuBisCO makes direct, physical contact with the lower section of two *cis* apical domains in the region of Phe 281, a segment of the inner apical domain previously identified as important for substrate protein encapsulation and folding (Fenton et al., 1994). Simultaneous binding of the nonnative substrate protein by both the C-terminal tails and the lower segment of the *cis* apical domains could thus provide a mechanism for retaining the nonnative substrate protein while the GroEL ring shifts into the R2 state to permit loading of GroES.

How GroES makes initial contact with a GroEL ring already occupied by a large and bulky nonnative substrate protein remains unclear. The earliest stages of the encapsulation reaction undoubtedly follow an ATP-driven elevation and movement of the GroEL apical domains, structural shifts that are capable of mechanically unfolding the bound substrate protein (Clare et al., 2012; Lin et al., 2008). However, only a subset of the apical domains must maintain contact with the nonnative protein during the encapsulation reaction (Farr et al., 2000). This observation suggests that, in the earliest stages of contact between GroES and a substrate-occupied GroEL ring, apical domains not in direct contact with the substrate protein are the ones employed to initially capture GroES. Such a loading mechanism would likely require that the cooperative interactions between the apical domains in the R2 *cis* ring be relaxed or partially uncoupled, in order for different apical domains to bind to two distinct ligands in different positions. In support of this idea, we find that the substrate-occupied EL43Py398A-GroES complex breaks C7 rotational symmetry (Figures 4A–4C).

Effects of Nonnative Substrate Protein on Inter-ring Allostery

Whereas changes in the *cis* ring complex are essential for the progression of the GroEL folding cycle, the *trans* ring also plays a central role. Substrate proteins first enter the GroEL reaction cycle on the open *trans* ring of the asymmetric GroEL-GroES complex, and the nucleotide state of each ring directly influences the functional state of the other ring (Horovitz et al., 2001; Lin et al., 2008; Rye et al., 1997; Sparrer and Buchner, 1997). For example, the presence of ATP on one ring inhibits ATP binding to the other ring (negative cooperativity) and the presence of ADP on one ring, while permitting ATP to bind to the second ring, nonetheless noncompetitively inhibits ATP hydrolysis on the other ring (Burston et al., 1995; Kad et al., 1998; Yifrach and Horovitz, 1995). These *trans* ring effects are thought to be essential for imposing the ring-ring asymmetry needed for the GroEL-GroES machine to function as a two-stroke motor (Burston et al., 1995; Frank et al., 2010; Kad et al., 1998; Rye et al., 1999; Yifrach and Horovitz, 2000). Whereas the structural nature of this ring-ring allostery remains incompletely understood, our flexible fitting analysis of different GroEL-GroES complexes provides insight into structural changes imposed on the *trans* ring by the ligand status of the *cis* ring.

The occupancy of a *cis* ring R2 cavity by nonnative RuBisCO appears to be communicated to the *trans* ring through substantial and asymmetric displacements of the *trans* ring apical domains (Figures 7C, 7F, and S3B). The apical domains of the R2 complex *trans* ring appear to be drawn inward, resulting in a smaller ring opening (Figures 7C and 7F). This change involves both counterclockwise rotations and outward tilting of the *trans*-ring apical domains (Figures 7C and 7F), resulting in a reordering the cavity-facing apical surface. Interestingly, the conformational shift of the *trans* ring is different in detail when RuBisCO is present in the *cis* cavity, with the magnitude of the apical domain movement in the *trans* ring being considerably larger and the extent of domain rotation being much smaller (Figures 7C and 7F). The observed closing down of the *trans*-ring opening in the R2 complex, both with and without nonnative protein in the *cis* cavity, could provide a mechanism to prevent nonnative substrate proteins from binding to the *trans* ring until the substrate protein inside the *cis* complex is committed to release and folding.

A Model for Substrate Protein Encapsulation, Release, and Folding

The observations described here thus suggest a multistep model for substrate protein encapsulation, release, and folding. Initial capture of a nonnative substrate protein on the apical face of a GroEL ring is accompanied by additional binding contacts between the substrate protein and the C-terminal tails of the GroEL subunits. Subsequent binding of ATP to the GroEL ring initiates the movement of the GroEL apical domains, weakening the interaction between the nonnative substrate protein and the apical domains (Badcoe et al., 1991; Martin et al., 1991; Viitanen et al., 1991). Binding contacts between the nonnative substrate protein and the C-terminal tails at the base of the cavity serve to reduce the probability of premature substrate protein escape as the apical domains move to accommodate GroES. Our structural analysis of the EL43Py398A complexes further suggests that population of the GroES acceptor state (the R2 state) requires an intermediate arrangement of the GroEL apical domains (Figure 7). The consequence of this altered apical position involves a shift in the binding position of the GroES heptamer and the simultaneous exposure of a partial binding surface for the nonnative substrate protein at the bottom of the apical domains (Figure 7). A subsequent allosteric transition of the GroEL-GroES cavity to the R3 state of the ring then results in a shift of the apical domains to their high-affinity state for GroES, fully occluding the apical binding surface and ejecting the nonnative substrate protein from the apical face (Cliff et al., 2006; Madan et al., 2008; Ueno et al., 2004). Coordinated movements in the C-terminal regions of the equatorial domains serve to draw the C-terminal tails away from the substrate protein, resulting in full release of the nonnative substrate protein and the initiation of folding. However, this release from the C termini does not appear to be total, as the C-terminal tails continue to make ongoing, though reduced, physical contacts with the substrate protein following release and the initiation of folding (Figure 5). Whether these ongoing contacts directly influence the folding of a substrate protein remains to be determined.

EXPERIMENTAL PROCEDURES

Full details of the experimental procedures can be found in the Extended Experimental Procedures.

Proteins

Wild-type GroEL, EL398A, EL43C, and EL43C398A were expressed and purified as previously described (Lin et al., 2008). ELΔ526 was purified in the same manner as wild-type GroEL. GroES, RuBisCO, and GFP were also expressed and purified as previously described (Lin and Rye, 2006; Lin et al., 2008; Rye et al., 1997, 1999). Bovine rhodanese was purchased from Sigma-Aldrich and purified as previously described (Madan et al., 2008; Weissman et al., 1994).

Labeling of Proteins with Fluorescent Dyes

EL43C and EL43C398A were specifically labeled at Cys43 with the thiol-reactive dye N-1-pyrene maleimide (PM) to generate EL43Py and EL43Py398A as previously described (Madan et al., 2008). Wild-type RuBisCO was fluorescently labeled at Cys58 with the thiol-reactive dye 5-iodoacetamidofluorescein (5IAF) to create 58F-RuBisCO as previously described (Lin and Rye, 2006; Lin et al., 2008; Rye et al., 1999). Both PM and 5IAF were obtained from Invitrogen (Molecular Probes, Eugene, OR, USA) and prepared fresh from dry powder in anhydrous DMF immediately prior to use. The extent and specificity of dye conjugation was confirmed as previously described (Lin and Rye, 2004; Lin et al., 2008; Rye, 2001). For 58F-RuBisCO, EL43Py, and EL43Py398A, the labeling efficiency was confirmed to be 98%–100% by at least two different methods of analysis (Madan et al., 2008; Rye, 2001).

Refolding, Enzymatic, and Encapsulation Assays

Encapsulation experiments were conducted in sample buffer: 50 mM HEPES (pH 7.6), 15 mM $Mg(OAc)_2$, 100 mM KOAc, and 2 mM DTT. Substrate protein (58F-RuBisCO, GFP, or rhodanese) was denatured in acid urea buffer for 30–60 min at room temperature (in the dark) to yield working stocks of dRub, dGFP, and dRho. ADP bullet complexes (Lin et al., 2008) with nonnative GFP, rhodanese, or RuBisCO bound to the *trans* ring were formed by adding dGFP, dRho, or dRub to ADP bullets at a mixing stoichiometry of 1:1 in cold buffer. After 5 min at room temperature, ATP was added to permit GroES binding and protein encapsulation and then quenched by addition of hexokinase and glucose. The complex mixture was separated on a Superose 6 gel filtration column, equilibrated in sample buffer, and supplemented with 50 μM ADP, connected to an in-line fluorescence detector. For experiments with GFP and RuBisCO, captured protein was quantified using in-line fluorescence detection. For experiments with rhodanese, the GroEL-GroES peak was collected, and encapsulated rhodanese was quantified by SDS-PAGE and densitometry (see the Extended Experimental Procedures).

Cryo-EM and Data Processing

The freezing of chaperonin samples for cryo-EM was done in accordance with the standard method (see the Extended Experimental Procedures). Electron images of frozen, hydrated specimens were recorded at 300 kV in either JEM-3000SFF or JEM-3200FSC cryo-electron microscopes on photographic films or CCD camera (see the Extended Experimental Procedures). The digital images were preprocessed by boxing particle images and determining contrast transfer function parameters for each micrograph using EMAN1 program (Ludtke et al., 1999).

The methodology of EMAN1 multiple-model refinement (multirefine) for compositionally and conformationally heterogeneous complex analysis, which has been previously described (Chen et al., 2006), was used to sort different particle subpopulations from all the data sets (Figure S7A). Here, several consecutive multiple-model refinements were applied to "purify" the relatively homogeneous bullet-shaped particle images of greatest interest for each of three complexes described in this study (see the Extended Experimental Procedures). Each subpopulation with "purified" particle images was subject to a single-model refinement (refine) to obtain a final converged bullet-shaped 3D reconstruction. The Euler angular distributions of particle images corresponding to each of the reconstructions (Figures 2A, 3A, and 5A) are shown in Figures S7B–S7D, respectively.

The final resolutions for the refined structures were assessed using the gold-standard criterion of Fourier Shell Correlation (FSC) cutoff at 0.143 from two independent half-sets of data (Scheres and Chen, 2012) after the particle images were highly purified from our consecutive multiple-model refinement procedures. Chimera (Pettersen et al., 2004) was used for the surface representations of all the cryo-EM density maps. The 3D variance map of the EL43Py398A-RuBisCO-GroES-ATP complex was calculated using the EMAN1 program calculateMapVariance.py with the bootstrap technique implemented (Chen et al., 2008; Penczek et al., 2006).

Fitting of X-Ray Structure into Cryo-EM Density Maps

To standardize the pixel size of the substrate occupied and empty density maps of the GroEL-GroES complexes, a number of density maps were generated with different pixel sizes between 2.0 and 2.2 Å because different electron microscopes and recording media were used. The X-ray structure of the GroEL-GroES-ADP complex (PDB ID code 1AON) was then refined against each of these density maps using *DireX* (Schröder et al., 2007). As the orientation of the equatorial domains in the density maps was very similar to the X-ray structure, we used those domains as reference regions for magnification calibration for each map. The root-mean-square deviation (RMSD) between all equatorial domains of the fitted models and the X-ray structure of the GroEL-GroES-ADP complex was calculated, and the optimal pixel size was chosen as the one that leads to the smallest RMSD value. The optimized pixel sizes for the three density maps of the EL43Py398A-GroES-ATP, EL43Py398A-RuBisCO-GroES-ATP, and EL398A-RuBisCO-GroES-ATP complexes were 2.08, 2.04, and 2.12 Å, respectively.

The GroEL-GroES-ADP crystal structure (PDB ID code 1AON) was fitted as a rigid body into the density maps of the EL43Py398A-GroES-ATP, EL43Py398A-RuBisCO-GroES-ATP, EL398A-RuBisCO-GroES-ATP, and EL398A-GroES-ATP complexes. This rigidly docked structure served as the starting point for our strongly restrained flexible fitting using the program DireX (Schröder et al., 2007).

ACCESSION NUMBERS

The cryo-EM density maps for EL43Py398A-GroES-ATP complex, EL43Py398A-RuBisCO-GroES-ATP complex, and EL398A-RuBisCO-GroES-ATP complex are deposited to the Electron Microscopy Data Bank with accession numbers EMD-2325, EMD-2326, and EMD-2327, respectively. The fitted models are deposited in the Protein Data Bank under ID codes 3zpz, 3zq0, and 3zq1, respectively.

SUPPLEMENTAL INFORMATION

Supplemental Information includes Extended Experimental Procedures and seven figures and can be found with this article online at http://dx.doi.org/10.1016/j.cell.2013.04.052.

ACKNOWLEDGMENTS

This research has been supported by grants from the National Institutes of Health (P41GM103832 and PN2EY016525 to W.C.) (GM065421 to H.S.R.). We would like to thank Dr. Chavela Carr for her comments on the manuscript and Dr. Steven J. Ludtke and Dr. Michael F. Schmid for helpful discussions.

Received: July 27, 2012
Revised: January 6, 2013
Accepted: April 19, 2013
Published: June 6, 2013

REFERENCES

Badcoe, I.G., Smith, C.J., Wood, S., Halsall, D.J., Holbrook, J.J., Lund, P., and Clarke, A.R. (1991). Binding of a chaperonin to the folding intermediates of lactate dehydrogenase. Biochemistry *30*, 9195–9200.

Baker, M.L., Ju, T., and Chiu, W. (2007). Identification of secondary structure elements in intermediate-resolution density maps. Structure *15*, 7–19.

Braig, K., Otwinowski, Z., Hegde, R., Boisvert, D.C., Joachimiak, A., Horwich, A.L., and Sigler, P.B. (1994). The crystal structure of the bacterial chaperonin GroEL at 2.8 A. Nature *371*, 578–586.

Burston, S.G., Ranson, N.A., and Clarke, A.R. (1995). The origins and consequences of asymmetry in the chaperonin reaction cycle. J. Mol. Biol. *249*, 138–152.

Chen, S., Roseman, A.M., Hunter, A.S., Wood, S.P., Burston, S.G., Ranson, N.A., Clarke, A.R., and Saibil, H.R. (1994). Location of a folding protein and shape changes in GroEL-GroES complexes imaged by cryo-electron microscopy. Nature *371*, 261–264.

Chen, D.H., Song, J.L., Chuang, D.T., Chiu, W., and Ludtke, S.J. (2006). An expanded conformation of single-ring GroEL-GroES complex encapsulates an 86 kDa substrate. Structure *14*, 1711–1722.

Chen, D.-H., Luke, K., Zhang, J., Chiu, W., and Wittung-Stafshede, P. (2008). Location and flexibility of the unique C-terminal tail of Aquifex aeolicus co-chaperonin protein 10 as derived by cryo-electron microscopy and biophysical techniques. J. Mol. Biol. *381*, 707–717.

Clare, D.K., Bakkes, P.J., van Heerikhuizen, H., van der Vies, S.M., and Saibil, H.R. (2009). Chaperonin complex with a newly folded protein encapsulated in the folding chamber. Nature *457*, 107–110.

Clare, D.K., Vasishtan, D., Stagg, S., Quispe, J., Farr, G.W., Topf, M., Horwich, A.L., and Saibil, H.R. (2012). ATP-triggered conformational changes delineate substrate-binding and -folding mechanics of the GroEL chaperonin. Cell *149*, 113–123.

Cliff, M., Limpkin, C., Cameron, A., Burston, S., and Clarke, A. (2006). Elucidation of steps in the capture of a protein substrate for efficient encapsulation by GroE. J. Biol. Chem. *281*, 21266–21275.

Cong, Y., Schröder, G.F., Meyer, A.S., Jakana, J., Ma, B., Dougherty, M.T., Schmid, M.F., Reissmann, S., Levitt, M., Ludtke, S.L., et al. (2012). Symmetry-free cryo-EM structures of the chaperonin TRiC along its ATPase-driven conformational cycle. EMBO J. *31*, 720–730.

Elad, N., Farr, G.W., Clare, D.K., Orlova, E.V., Horwich, A.L., and Saibil, H.R. (2007). Topologies of a substrate protein bound to the chaperonin GroEL. Mol. Cell *26*, 415–426.

Falke, S., Tama, F., Brooks, C.L., 3rd, Gogol, E.P., and Fisher, M.T. (2005). The 13 angstroms structure of a chaperonin GroEL-protein substrate complex by cryo-electron microscopy. J. Mol. Biol. *348*, 219–230.

Farr, G.W., Furtak, K., Rowland, M.B., Ranson, N.A., Saibil, H.R., Kirchhausen, T., and Horwich, A.L. (2000). Multivalent binding of nonnative substrate proteins by the chaperonin GroEL. Cell *100*, 561–573.

Farr, G.W., Fenton, W.A., and Horwich, A.L. (2007). Perturbed ATPase activity and not "close confinement" of substrate in the *cis* cavity affects rates of folding by tail-multiplied GroEL. Proc. Natl. Acad. Sci. USA *104*, 5342–5347.

Fenton, W.A., Kashi, Y., Furtak, K., and Horwich, A.L. (1994). Residues in chaperonin GroEL required for polypeptide binding and release. Nature *371*, 614–619.

Frank, G.A., Goomanovsky, M., Davidi, A., Ziv, G., Horovitz, A., and Haran, G. (2010). Out-of-equilibrium conformational cycling of GroEL under saturating ATP concentrations. Proc. Natl. Acad. Sci. USA *107*, 6270–6274.

Grason, J.P., Gresham, J.S., and Lorimer, G.H. (2008). Setting the chaperonin timer: a two-stroke, two-speed, protein machine. Proc. Natl. Acad. Sci. USA *105*, 17339–17344.

Hartl, F.U., Bracher, A., and Hayer-Hartl, M. (2011). Molecular chaperones in protein folding and proteostasis. Nature *475*, 324–332.

Horovitz, A., Fridmann, Y., Kafri, G., and Yifrach, O. (2001). Review: allostery in chaperonins. J. Struct. Biol. *135*, 104–114.

Horwich, A.L., and Fenton, W.A. (2009). Chaperonin-mediated protein folding: using a central cavity to kinetically assist polypeptide chain folding. Q. Rev. Biophys. *42*, 83–116.

Kad, N.M., Ranson, N.A., Cliff, M.J., and Clarke, A.R. (1998). Asymmetry, commitment and inhibition in the GroE ATPase cycle impose alternating functions on the two GroEL rings. J. Mol. Biol. *278*, 267–278.

Kanno, R., Koike-Takeshita, A., Yokoyama, K., Taguchi, H., and Mitsuoka, K. (2009). Cryo-EM structure of the native GroEL-GroES complex from thermus thermophilus encapsulating substrate inside the cavity. Structure *17*, 287–293.

Lin, Z., and Rye, H.S. (2004). Expansion and compression of a protein folding intermediate by GroEL. Mol. Cell *16*, 23–34.

Lin, Z., and Rye, H.S. (2006). GroEL-mediated protein folding: making the impossible, possible. Crit. Rev. Biochem. Mol. Biol. *41*, 211–239.

Lin, Z., Madan, D., and Rye, H.S. (2008). GroEL stimulates protein folding through forced unfolding. Nat. Struct. Mol. Biol. *15*, 303–311.

Ludtke, S.J., Baldwin, P.R., and Chiu, W. (1999). EMAN: semiautomated software for high-resolution single-particle reconstructions. J. Struct. Biol. *128*, 82–97.

Machida, K., Kono-Okada, A., Hongo, K., Mizobata, T., and Kawata, Y. (2008). Hydrophilic residues 526 KNDAAD 531 in the flexible C-terminal region of the chaperonin GroEL are critical for substrate protein folding within the central cavity. J. Biol. Chem. *283*, 6886–6896.

Madan, D., Lin, Z., and Rye, H.S. (2008). Triggering protein folding within the GroEL-GroES complex. J. Biol. Chem. *283*, 32003–32013.

Martin, J., Langer, T., Boteva, R., Schramel, A., Horwich, A.L., and Hartl, F.U. (1991). Chaperonin-mediated protein folding at the surface of groEL through a 'molten globule'-like intermediate. Nature *352*, 36–42.

Mayhew, M., da Silva, A.C., Martin, J., Erdjument-Bromage, H., Tempst, P., and Hartl, F.U. (1996). Protein folding in the central cavity of the GroEL-GroES chaperonin complex. Nature *379*, 420–426.

McLennan, N.F., Girshovich, A.S., Lissin, N.M., Charters, Y., and Masters, M. (1993). The strongly conserved carboxyl-terminus glycine-methionine motif of the Escherichia coli GroEL chaperonin is dispensable. Mol. Microbiol. *7*, 49–58.

Penczek, P.A., Yang, C., Frank, J., and Spahn, C.M.T. (2006). Estimation of variance in single-particle reconstruction using the bootstrap technique. J. Struct. Biol. *154*, 168–183.

Pettersen, E.F., Goddard, T.D., Huang, C.C., Couch, G.S., Greenblatt, D.M., Meng, E.C., and Ferrin, T.E. (2004). UCSF Chimera—a visualization system for exploratory research and analysis. J. Comput. Chem. *25*, 1605–1612.

Ranson, N.A., Clare, D.K., Farr, G.W., Houldershaw, D., Horwich, A.L., and Saibil, H.R. (2006). Allosteric signaling of ATP hydrolysis in GroEL-GroES complexes. Nat. Struct. Mol. Biol. *13*, 147–152.

Roseman, A.M., Chen, S., White, H., Braig, K., and Saibil, H.R. (1996). The chaperonin ATPase cycle: mechanism of allosteric switching and movements of substrate-binding domains in GroEL. Cell *87*, 241–251.

Rye, H.S. (2001). Application of fluorescence resonance energy transfer to the GroEL-GroES chaperonin reaction. Methods *24*, 278–288.

Rye, H.S., Burston, S.G., Fenton, W.A., Beechem, J.M., Xu, Z., Sigler, P.B., and Horwich, A.L. (1997). Distinct actions of *cis* and *trans* ATP within the double ring of the chaperonin GroEL. Nature *388*, 792–798.

Rye, H.S., Roseman, A.M., Chen, S., Furtak, K., Fenton, W.A., Saibil, H.R., and Horwich, A.L. (1999). GroEL-GroES cycling: ATP and nonnative polypeptide direct alternation of folding-active rings. Cell *97*, 325–338.

Scheres, S.H.W., and Chen, S. (2012). Prevention of overfitting in cryo-EM structure determination. Nat. Methods *9*, 853–854.

Schröder, G.F., Brunger, A.T., and Levitt, M. (2007). Combining efficient conformational sampling with a deformable elastic network model facilitates structure refinement at low resolution. Structure *15*, 1630–1641.

Sparrer, H., and Buchner, J. (1997). How GroES regulates binding of nonnative protein to GroEL. J. Biol. Chem. *272*, 14080–14086.

Tang, Y.C., Chang, H.C., Roeben, A., Wischnewski, D., Wischnewski, N., Kerner, M.J., Hartl, F.U., and Hayer-Hartl, M. (2006). Structural features of the GroEL-GroES nano-cage required for rapid folding of encapsulated protein. Cell *125*, 903–914.

Todd, M.J., Viitanen, P.V., and Lorimer, G.H. (1994). Dynamics of the chaperonin ATPase cycle: implications for facilitated protein folding. Science *265*, 659–666.

Ueno, T., Taguchi, H., Tadakuma, H., Yoshida, M., and Funatsu, T. (2004). GroEL mediates protein folding with a two successive timer mechanism. Mol. Cell *14*, 423–434.

van der Vies, S.M., Viitanen, P.V., Gatenby, A.A., Lorimer, G.H., and Jaenicke, R. (1992). Conformational states of ribulosebisphosphate carboxylase and their interaction with chaperonin 60. Biochemistry *31*, 3635–3644.

Viitanen, P.V., Donaldson, G.K., Lorimer, G.H., Lubben, T.H., and Gatenby, A.A. (1991). Complex interactions between the chaperonin 60 molecular chaperone and dihydrofolate reductase. Biochemistry *30*, 9716–9723.

Weissman, J.S., Kashi, Y., Fenton, W.A., and Horwich, A.L. (1994). GroEL-mediated protein folding proceeds by multiple rounds of binding and release of nonnative forms. Cell *78*, 693–702.

Weissman, J.S., Hohl, C.M., Kovalenko, O., Kashi, Y., Chen, S., Braig, K., Saibil, H.R., Fenton, W.A., and Horwich, A.L. (1995). Mechanism of GroEL action: productive release of polypeptide from a sequestered position under GroES. Cell *83*, 577–587.

Weissman, J.S., Rye, H.S., Fenton, W.A., Beechem, J.M., and Horwich, A.L. (1996). Characterization of the active intermediate of a GroEL-GroES-mediated protein folding reaction. Cell *84*, 481–490.

Xu, Z., Horwich, A.L., and Sigler, P.B. (1997). The crystal structure of the asymmetric GroEL-GroES-(ADP)7 chaperonin complex. Nature *388*, 741–750.

Yifrach, O., and Horovitz, A. (1995). Nested cooperativity in the ATPase activity of the oligomeric chaperonin GroEL. Biochemistry *34*, 5303–5308.

Yifrach, O., and Horovitz, A. (2000). Coupling between protein folding and allostery in the GroE chaperonin system. Proc. Natl. Acad. Sci. USA *97*, 1521–1524.